



A numerical scheme for regularized anisotropic curve shortening flow

Frank Haußer*, Axel Voigt

Crystal Growth Group, Research Center caesar, Ludwig-Erhard-Allee 2, 53175 Bonn, Germany

Received 8 December 2003; accepted 12 May 2005

Abstract

Realistic interfacial energy densities are often non-convex, which results in backward parabolic behavior of the corresponding anisotropic curve shortening flow, thereby inducing phenomena such as the formation of corners and facets. Adding a term that is quadratic in the curvature to the interfacial energy yields a regularized evolution equation for the interface, which is fourth-order parabolic. Using a semi-implicit time discretization, we present a variational formulation of this equation, which allows the use of linear finite elements. The resulting linear system is shown to be uniquely solvable. We also present numerical examples.

© 2005 Elsevier Ltd. All rights reserved.

MSC: 35K55; 65M12; 65M15; 65M60

Keywords: Mean curvature flow; Willmore flow; Fourth-order equations; Parametric finite elements; Anisotropy; Wulff shape; Faceting

1. Introduction

The evolution of interfaces is of great importance in many physical processes, including phase transitions, epitaxial growth and the evolution of grain boundaries. One of the earliest theories describing a purely interface-controlled evolution, i.e. independent of the behavior of the adjacent bulk phases, was

* Corresponding author.

E-mail addresses: hausser@caesar.de (F. Haußer), voigt@caesar.de (A. Voigt).

introduced in [1]. When appropriately scaled, the derived equation, today known as mean curvature flow – or curve shortening flow, if the interface is one dimensional – reads

$$v = -\kappa, \quad (1)$$

where v is the scalar normal velocity of the interface and κ its (mean) curvature. Eq. (1) is a second-order parabolic partial differential equation, which has been intensively studied in the past [2–5].

For one-dimensional interfaces, a generalization that encompasses an anisotropic interface energy density $\gamma(\phi)$, ϕ denoting the angle from a fixed axis to the unit normal \vec{n} of the interface Γ , reads

$$v = -\tilde{\gamma}\kappa, \quad \tilde{\gamma} = \gamma + \gamma''. \quad (2)$$

Here $\tilde{\gamma}\kappa$ is the anisotropic (mean) curvature, which may also be introduced formally as the first variation of the total interface energy

$$E_\gamma[\Gamma] = \int_\Gamma \gamma(\phi) d\Gamma.$$

Denoting with γ also the one-homogeneous extension on \mathbb{R}^2 , the Frank diagram \mathcal{F}_γ and the Wulff shape \mathcal{W}_γ of γ are defined as

$$\begin{aligned} \mathcal{F}_\gamma &= \{\vec{x} \in \mathbb{R}^2 \mid \gamma(\vec{x}) \leq 1\} \\ \mathcal{W}_\gamma &= \{\vec{x} \in \mathbb{R}^2 \mid \vec{x} \cdot \vec{n} \leq \gamma(\vec{n}) \forall \vec{n} \in \mathbb{R}^2, |\vec{n}| = 1\}. \end{aligned}$$

The Wulff shape denotes the equilibrium shape of the interface according to the introduced anisotropic energy. It is well known that $\tilde{\gamma}$ is strictly positive iff the Frank diagram is convex or iff γ is a convex function on \mathbb{R}^2 . In this case, (2) is parabolic and well behaved; for a theoretical treatment see [3,6]. But crystalline materials are often endowed with interfacial energies which are not convex; see [7,8]. Such energies may lead to corners, facets and wrinklings of the Wulff shape \mathcal{W}_γ and turn Eq. (2) into a backward parabolic equation within non-convex ranges of γ . One way to overcome this inherently unstable behavior is to regularize the equation by adding a curvature dependent term to the interface energy density, which was already proposed on physical grounds in [7]. As introduced in [9], choosing an interfacial energy

$$\gamma + \frac{1}{2}\epsilon\kappa^2,$$

with $\epsilon > 0$ constant, leads to the highly nonlinear fourth-order parabolic evolution equation

$$v = -\tilde{\gamma}\kappa + \epsilon \left(\partial_{ss}\kappa + \frac{1}{2}\kappa^3 \right), \quad (3)$$

where ∂_{ss} denotes the second tangential derivative along the interface. This problem is similar to the evolution of elastic curves, which has been examined both from a theoretical and numerical point of view in [10].

In Section 2 we derive a finite element discretization of Eq. (3) using methods similar to those in [11–13]. We start with reformulating Eq. (3) as a system of second-order equations. Using a semi-implicit time discretization, we will derive a variational formulation of this system, which allows a finite element discretization in space using parametric linear finite elements. A Schur complement approach is used to solve the resulting linear system. In Section 3, we present some numerical results.

2. Variational formulation and finite element discretization

Introducing the position vector \vec{x} , the curvature vector $\vec{\kappa} = \kappa \vec{n}$, and the velocity vector $\vec{v} = v \vec{n}$, and using the geometric expression $\vec{\kappa} = -\partial_{s,s} \vec{x}$, Eq. (3) becomes equivalent to the following system of equations for $\vec{\kappa}$, κ , v , and \vec{v} :

$$\vec{\kappa} = -\partial_{s,s} \vec{x}, \tag{4}$$

$$\kappa = \vec{\kappa} \cdot \vec{n}, \tag{5}$$

$$v = -\tilde{\gamma} \kappa + \epsilon \left(\partial_{s,s} \kappa + \frac{1}{2} \kappa^3 \right), \tag{6}$$

$$\vec{v} = v \vec{n}. \tag{7}$$

Let $\Gamma(t)$ denote the interface at time t . Now split the time interval using discrete time instants $0 = t_0 < t_1 < \dots$ and define time steps $\tau_m := t_{m+1} - t_m$. We represent the next interface $\Gamma^{m+1} = \Gamma(t_{m+1})$ in terms of $\Gamma^m = \Gamma(t_m)$ by updating the position vector

$$\vec{x}^{m+1} \leftarrow \vec{x}^m + \tau_m \vec{v}. \tag{8}$$

In the time discretization, all geometric quantities such as \vec{n} and $\partial_{s,s}$ are evaluated on the current interface Γ^m . In contrast to the geometric quantities, the unknowns $\vec{\kappa}$, κ , v , and \vec{v} are treated implicitly, with the exception of the nonlinear term κ^3 which is treated semi-implicitly, i.e. $\kappa^3 = \kappa^{m+1} (\kappa^m)^2$. In particular, in view of (8), we define

$$\vec{\kappa}^{m+1} = -\partial_{s,s} (\vec{x}^m + \tau_m \vec{v}^{m+1}). \tag{9}$$

To derive a weak formulation, we proceed as in [11,13,14]: multiply (5)–(7) and (9) by test functions $\vec{\psi} \in \vec{H}^1(\Gamma)$ and $\psi \in H^1(\Gamma)$, and use integration by parts for the second-order operator $\partial_{s,s}$. For simplicity, we have hereafter dropped the superscript $m + 1$ for the unknowns $\vec{\kappa}^{m+1}$, etc. Furthermore, using the notation $\langle \cdot, \cdot \rangle$ for the L^2 inner product over the current interface Γ^m , we arrive at the following set of semi-implicit equations:

Problem 1. For $m = 1, 2, \dots$ find $\vec{\kappa} \in \vec{H}^1(\Gamma^m)$, $\kappa \in H^1(\Gamma^m)$, $v \in H^1(\Gamma^m)$, and $\vec{v} \in \vec{H}^1(\Gamma^m)$ such that $\forall \psi \in H^1(\Gamma^m)$ and $\forall \vec{\psi} \in \vec{H}^1(\Gamma^m)$,

$$\langle \vec{\kappa}, \vec{\psi} \rangle - \tau_m \langle \partial_s \vec{v}, \partial_s \vec{\psi} \rangle = \langle \partial_s \vec{x}^m, \partial_s \vec{\psi} \rangle,$$

$$\langle \kappa, \psi \rangle - \langle \vec{\kappa} \cdot \vec{n}, \psi \rangle = 0,$$

$$\langle v, \psi \rangle + \langle \tilde{\gamma} \kappa, \psi \rangle + \epsilon \langle \partial_s \kappa, \partial_s \psi \rangle - \frac{1}{2} \epsilon \langle (\kappa^m)^2 \kappa, \psi \rangle = 0,$$

$$\langle \vec{v}, \vec{\psi} \rangle - \langle v \vec{n}, \vec{\psi} \rangle = 0.$$

Now the discretization in space is straightforward. Consider a polygonal curve Γ_h^m approximating Γ^m . The polygonal segments are thought of as finite elements. Also for the polygonal curve, we denote by \vec{n} the outer unit normal to Γ_h^m , which may be discontinuous across inter-element boundaries. Denote by $\mathbb{W}_h^m \subseteq H^1(\Gamma_h^m)$ the finite element space of globally continuous, piecewise linear functions with corresponding nodal basis functions $(\psi_l)_{l=1}^L$, where L is the number of degrees of freedom. By $\vec{\mathbb{W}}_h^m \subseteq \vec{H}^1(\Gamma_h^m)$ we denote the finite element space of vector valued functions with nodal basis functions $(\vec{\psi}_l^q)_{l=1, \dots, L}^{q=1, 2}$, where $\vec{\psi}_l^q = \psi_l \vec{e}_q$ with ψ_l the scalar basis function defined above and (\vec{e}_1, \vec{e}_2) the standard basis in \mathbb{R}^2 . Problem 1 is discretized by expanding the functions $\vec{\kappa}$, κ , v , \vec{v} in terms of the basis functions

and testing against all discrete test functions, i.e. solving **Problem 1** in the finite dimensional spaces $\mathbb{W}_h^m, \bar{\mathbb{W}}_h^m$.

To arrive at an algorithm in matrix form, expand the unknowns

$$\vec{\kappa}_h = \sum_{l=1}^L \vec{K}_l \psi_l, \quad \kappa_h = \sum_{l=1}^L K_l \psi_l, \quad \vec{v}_h = \sum_{l=1}^L \vec{V}_l \psi_l, \quad v_h = \sum_{l=1}^L V_l \psi_l$$

for some

$$\vec{K} = (\vec{K}_1, \dots, \vec{K}_L)^t \in \mathbb{R}^{2 \times L}, \quad L = (K_1, \dots, K_L)^t \in \mathbb{R}^L$$

$$\vec{V} = (\vec{V}_1, \dots, \vec{V}_L)^t \in \mathbb{R}^{2 \times L}, \quad V = (V_1, \dots, V_L)^t \in \mathbb{R}^L$$

and define the mass, stiffness, and normal matrices:

$$\mathbf{M} = (M_{kl}), \quad M_{kl} = \langle \psi_k, \psi_l \rangle; \quad \vec{\mathbf{M}} = (\vec{M}_{kl}), \quad \vec{M}_{kl} = (M_{kl}^{qr}) = (\delta_{qr} M_{kl})$$

$$\mathbf{A} = (A_{kl}), \quad A_{kl} = \langle \partial_s \psi_k, \partial_s \psi_l \rangle; \quad \vec{\mathbf{A}} = (\vec{A}_{kl}), \quad \vec{A}_{kl} = (A_{kl}^{qr}) = (\delta_{qr} A_{kl})$$

$$\mathbf{M}_\gamma = (M_{\gamma,kl}), \quad M_{\gamma,kl} = \left\langle \left(\tilde{\gamma} - \frac{\epsilon}{2} (\kappa^m)^2 \right) \psi_k, \psi_l \right\rangle$$

$$\vec{\mathbf{N}} = (\vec{N}_{kl}), \quad \vec{N}_{kl} = (N_{kl}^q) = \langle \psi_k, \psi_l n^q \rangle$$

where the index ranges are $1 \leq k, l \leq L$ and $1 \leq q, r \leq 2$, $\delta_{qr} = \vec{e}_q \cdot \vec{e}_r$ is the Kronecker symbol, and $n^q = \vec{n} \cdot \vec{e}_q$ is the q -th spatial component of the normal.

The following algorithm is the matrix form of the discretized **Problem 1**:

Algorithm 2. Find $\vec{K}, \vec{V} \in \mathbb{R}^{2 \times L}, K, V \in \mathbb{R}^L$ such that

$$\begin{pmatrix} \vec{\mathbf{M}} & \mathbf{0} & \mathbf{0} & -\vec{\mathbf{N}} \\ \mathbf{0} & \mathbf{M} & -\vec{\mathbf{N}}^t & \mathbf{0} \\ -\tau_m \vec{\mathbf{A}} & \mathbf{0} & \vec{\mathbf{M}} & \mathbf{0} \\ \mathbf{0} & \mathbf{M}_\gamma + \epsilon \mathbf{A} & \mathbf{0} & \mathbf{M} \end{pmatrix} \begin{pmatrix} \vec{V} \\ K \\ \vec{K} \\ V \end{pmatrix} = \begin{pmatrix} 0 \\ 0 \\ \vec{\mathbf{A}} \vec{X}^m \\ 0 \end{pmatrix}.$$

A Schur complement equation for \vec{K}, V reads

$$\mathbf{S} \begin{pmatrix} \vec{K} \\ V \end{pmatrix} = \begin{pmatrix} \vec{\mathbf{A}} \vec{X}^m \\ 0 \end{pmatrix},$$

where

$$\mathbf{S} = \begin{pmatrix} \vec{\mathbf{M}} & \mathbf{0} \\ \mathbf{0} & \mathbf{M} \end{pmatrix} - \begin{pmatrix} -\tau_m \vec{\mathbf{A}} & \mathbf{0} \\ \mathbf{0} & \mathbf{M}_\gamma + \epsilon \mathbf{A} \end{pmatrix} \begin{pmatrix} \vec{\mathbf{M}} & \mathbf{0} \\ \mathbf{0} & \mathbf{M} \end{pmatrix}^{-1} \begin{pmatrix} \mathbf{0} & -\vec{\mathbf{N}} \\ -\vec{\mathbf{N}}^t & \mathbf{0} \end{pmatrix}$$

$$= \begin{pmatrix} \vec{\mathbf{M}} & -\tau_m \vec{\mathbf{A}} \vec{\mathbf{M}}^{-1} \vec{\mathbf{N}} \\ (\mathbf{M}_\gamma + \epsilon \mathbf{A}) \mathbf{M}^{-1} \vec{\mathbf{N}}^t & \mathbf{M} \end{pmatrix}.$$

The above formulation in turn gives rise to the final Schur complement equation for the single unknown V :

$$(\tau_m (\mathbf{M}_\gamma + \epsilon \mathbf{A}) \mathbf{M}^{-1} \vec{\mathbf{N}}^t \vec{\mathbf{M}}^{-1} \vec{\mathbf{A}} \vec{\mathbf{M}}^{-1} \vec{\mathbf{N}} + \mathbf{M}) V = -(\mathbf{M}_\gamma + \epsilon \mathbf{A}) \mathbf{M}^{-1} \vec{\mathbf{N}}^t \vec{\mathbf{M}}^{-1} \vec{\mathbf{A}} \vec{X}^m. \tag{10}$$

Once the scalar velocity V is obtained by solving Eq. (10), the unknown \vec{V} is easily computed by solving $\vec{M}\vec{V} = \vec{N}V$, and then \vec{X} is updated through

$$\vec{X} \leftarrow \vec{X} + \tau_m \vec{V}.$$

We would like to mention that the same algorithm may be used to describe the Willmore flow of curves. Indeed, choosing $\gamma(\phi) = 0$ and $\epsilon = 1$, Eq. (3) reduces to $v = \partial_{ss}\kappa + \frac{1}{2}\kappa^3$.

In order to show uniqueness of the discrete system it is sufficient to show that if $(\vec{\kappa}_h, \kappa_h, \vec{v}_h, v_h)$ satisfies

$$\langle \vec{\kappa}_h, \vec{\psi}_h \rangle - \tau_m \langle \partial_s \vec{v}_h, \partial_s \vec{\psi}_h \rangle = 0, \tag{11}$$

$$\langle \kappa_h, \psi_h \rangle - \langle \vec{\kappa}_h \cdot \vec{n}, \psi_h \rangle = 0, \tag{12}$$

$$\langle v_h, \psi_h \rangle + \langle \tilde{\gamma} \kappa_h, \psi_h \rangle + \epsilon \langle \partial_s \kappa_h, \partial_s \psi_h \rangle - \frac{1}{2} \epsilon \langle (\kappa_h^m)^2 \kappa_h, \psi_h \rangle = 0, \tag{13}$$

$$\langle \vec{v}_h, \vec{\psi}_h \rangle - \langle v_h \vec{n}, \vec{\psi}_h \rangle = 0, \tag{14}$$

then $(\vec{\kappa}_h, \kappa_h, \vec{v}_h, v_h) = 0$. Inserting $\vec{\psi}_h = \vec{\kappa}_h$ in (11) and using an inverse inequality one obtains

$$\|\vec{\kappa}_h\|_{L^2(\Gamma_h^m)}^2 \leq \tau_m \|\partial_s \vec{v}_h\|_{L^2(\Gamma_h^m)} \|\partial_s \vec{\kappa}_h\|_{L^2(\Gamma_h^m)} \leq C \tau_m h^{-2} \|\vec{v}_h\|_{L^2(\Gamma_h^m)} \|\vec{\kappa}_h\|_{L^2(\Gamma_h^m)},$$

where h is a lower bound on the lengths of the segments of Γ_h^m and C is a generic constant. With $\vec{\psi}_h = \vec{v}_h$ in (14) one gets $\|\vec{v}_h\|_{L^2(\Gamma_h^m)} \leq \|v_h\|_{L^2(\Gamma_h^m)}$ and therefore

$$\|\vec{\kappa}_h\|_{L^2(\Gamma_h^m)} \leq C \tau_m h^{-2} \|v_h\|_{L^2(\Gamma_h^m)}. \tag{15}$$

Using $\psi_h = v_h$ in (13) and applying again an inverse inequality one gets

$$\|v_h\|_{L^2(\Gamma_h^m)}^2 \leq C(1 + \epsilon h^{-2}) \|v_h\|_{L^2(\Gamma_h^m)} \|\kappa_h\|_{L^2(\Gamma_h^m)},$$

where we assume $\epsilon(\kappa^m)^2 \leq C$. With $\psi_h = \kappa_h$ in (12) one gets $\|\kappa_h\|_{L^2(\Gamma_h^m)} \leq \|\vec{\kappa}_h\|_{L^2(\Gamma_h^m)}$ and therefore

$$\|v_h\|_{L^2(\Gamma_h^m)} \leq C(1 + \epsilon h^{-2}) \|\vec{\kappa}_h\|_{L^2(\Gamma_h^m)}.$$

Inserting this into (15) yields $\vec{\kappa}_h = 0$ provided that $C \tau_m h^{-2} (1 + \epsilon h^{-2}) < 1$. This indicates that the parameters ϵ , τ_m and h may not be chosen independently of each other and the way in which they are related will certainly influence the stability of the scheme. In applications where faceting is modeled, ϵ is a small parameter and $\sqrt{\epsilon}$ sets the length scale of the rounded corners (see Section 3 for a numerical verification). In order to resolve this length scale we therefore need $h^2 \approx \epsilon$. This means that in practice we have a time step restriction $\tau_m \approx h^2$ (and not $\approx h^4$).

3. Implementation and results

We implement our numerical method using ALBERT, adaptive finite element software for scientific computation [15]. A simple (space) adaptive strategy is used. The one-dimensional finite element mesh for the initial interface consists of elements with almost uniform element size. This size is kept approximately constant during time evolution, i.e. in each time step, nodes are inserted or removed, if necessary. We note that adaptivity is indispensable for the algorithm to work in a parametric setting, since the fourth-order term tends to bring some nodes very close together! Alternatively mesh regularization

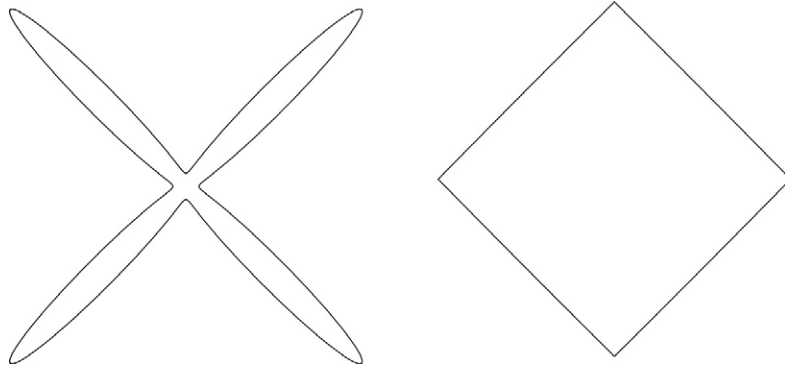


Fig. 1. Anisotropy $\gamma(\phi) = 1.0 + 0.9 \cos(4\phi)$; (left) Frank diagram \mathcal{F}_γ , (right) Wulff shape \mathcal{W}_γ .

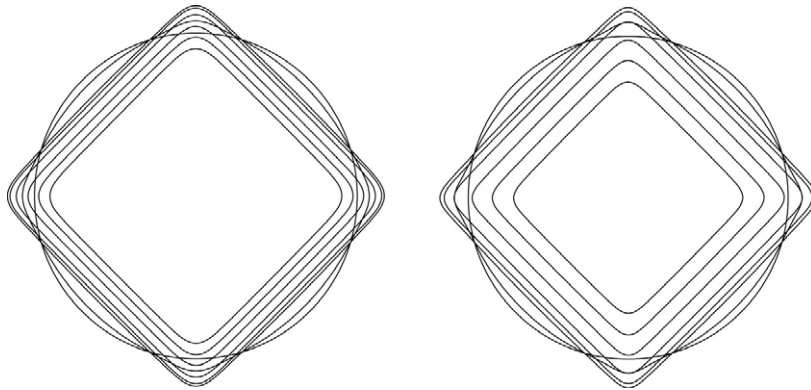


Fig. 2. Evolution under anisotropy $\gamma(\phi) = 1.0 + 0.9 \cos(4\phi)$, at time $t = 0, 0.1, 0.5, 2, 5, 10, 15, 20$; (left) $\epsilon = 1.0$, (right) $\epsilon = 0.5$.

may be used; see e.g. [11,16]. In order to test the algorithm, we chose a strongly non-convex anisotropy function:

$$\gamma(\phi) = 1.0 + 0.9 \cos(4\phi), \quad \text{i.e. } \tilde{\gamma}(\phi) = 1.0 - 13.5 \cos(4\phi), \quad (16)$$

which exhibits a fourfold symmetry. Fig. 1 shows the corresponding Frank diagram and the Wulff shape.

At $\phi = 0, \frac{1}{2}\pi, \pi, \frac{3}{2}\pi$ the convexified Frank diagram contains straight lines leading to the corners of the associated Wulff shape. We compute the regularized anisotropic curve shortening flow starting from a circle with radius $r = 5.0$ for different values of the parameter ϵ ; see Figs. 2 and 3. The time step is chosen to be $\tau_m = 10^{-5}$ and $h = 0.06$.

The time evolution of the flow depends on ϵ ; for decreasing ϵ the shrinking of the curve is enhanced. In all four cases the facets of the corresponding Wulff shape in Fig. 1 are approximated very well. Furthermore, as theoretically expected, it can be seen that $\sqrt{\epsilon}$ sets the length scale of the rounded corners; see Fig. 4. The zoom in the upper corner in this figure clearly demonstrates this introduced length scale.

For ϵ small enough, the solution becomes corrugated at the critical angles. This can be observed in Fig. 3 (right) and is further described in Fig. 5. The number of wrinkles which develop in the early stage of the evolution is related to the size of ϵ . These oscillations turn into “facets”. After the “facets” are built they tend to coarsen and lead to the final shape which corresponds to the Wulff shape.

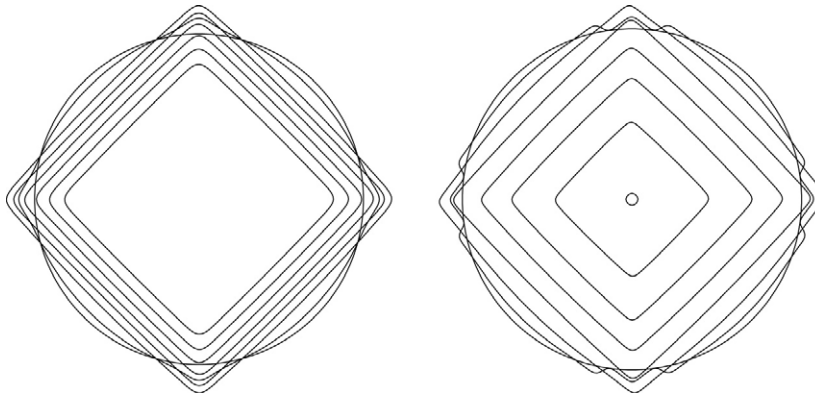


Fig. 3. Evolution under anisotropy $\gamma(\phi) = 1.0 + 0.9 \cos(4\phi)$, at time $t = 0, 0.1, 0.5, 2, 4, 6, 8, 10$; (left) $\epsilon = 0.25$, (right) $\epsilon = 0.1$.

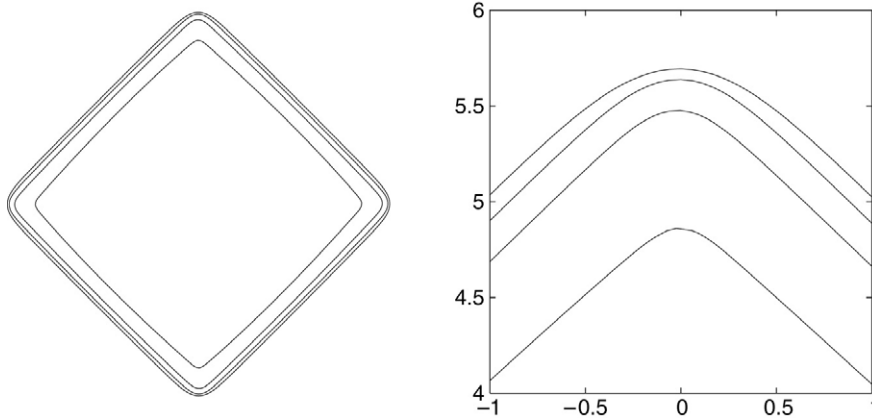


Fig. 4. Solutions at $t = 3.0$; from outer to inner curve: $\epsilon = 1.0, 0.5, 0.25, 0.1$; (left) whole shape, (right) zoom in the upper corner.

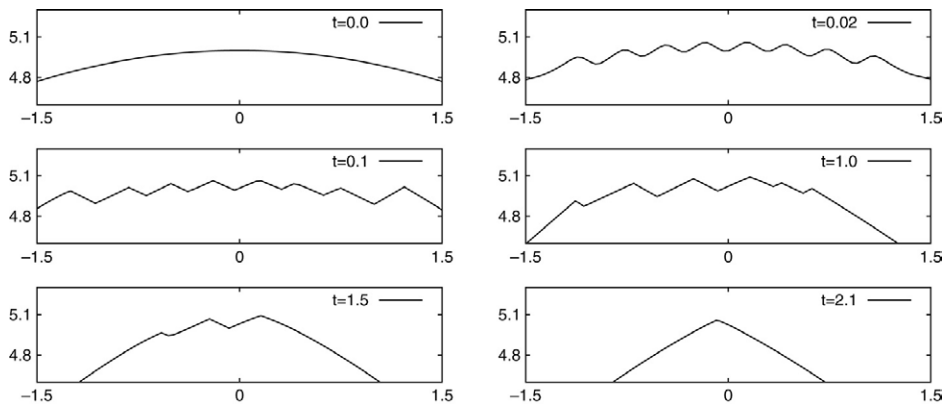


Fig. 5. Zoom for $\epsilon = 0.01$, $\tau_m = 10^{-5}$, $h = 0.03$.

Similar coarsening behavior has already been observed for a convective Cahn–Hilliard equation in [17]. The convective Cahn–Hilliard equation can be interpreted as a small slope approximation of the geometric evolution law studied, as was shown in [18]. A detailed analysis of the coarsening and the dependence of the time evolution on ϵ for the full geometric problem studied here will be given elsewhere.

Acknowledgments

We would like to thank Stephen J. Watson for bringing the regularization of anisotropic motion-by-curvature in [9] to our attention and one of our referees for correcting the proof of uniqueness of the discrete system.

References

- [1] W.W. Mullins, Two-dimensional motion of idealized grain boundaries, *J. Appl. Phys.* 27 (1956) 900–904.
- [2] J. Sethian, Curvature and the evolution of fronts, *Commun. Math. Phys.* 101 (1985) 487–499.
- [3] Y.G. Chen, Y. Giga, S. Goto, Uniqueness and existence of viscosity solutions of generalized mean curvature flow equations, *J. Differential Geom.* 33 (3) (1991) 749–786.
- [4] J.E. Taylor, J.W. Cahn, C.A. Handwerker, Geometric models of crystal growth, *Acta Metall. Mater.* 40 (7) (1992) 1443–1474.
- [5] K. Deckelnick, G. Dziuk, A fully discrete numerical scheme for weighted mean curvature flow, *Numer. Math.* 91 (2002) 423–452.
- [6] H.M. Soner, Motion of a set by the curvature of its boundary, *J. Differential Equations* 101 (2) (1993) 313–372.
- [7] C. Herring, Surface tension as a motivation for sintering, in: W.E. Kingston (Ed.), *The Physics of Powder Metallurgy*, McGraw-Hill, 1951.
- [8] J.W. Cahn, C.A. Handwerker, A vector thermodynamics for anisotropic surfaces. 2. Curved and faceted surfaces, *Acta Metall.* 22 (1974) 1205–1214.
- [9] A. Di Carlo, M.E. Gurtin, P. Podio-Guidugli, A regularized equation for anisotropic motion-by-curvature, *SIAM J. Appl. Math.* 52 (4) (1992) 1111–1119.
- [10] G. Dziuk, E. Kuwert, R. Schätzle, Evolution of elastic curves in \mathbb{R}^n : existence and computation, *SIAM J. Numer. Anal.* 33 (1999) 1228–1245.
- [11] E. Bänsch, P. Morin, R.H. Nochetto, Finite element methods for surface diffusion, in: A. Visintin, P. Colli, C. Verdi (Eds.), *Free Boundary Problems, Trento, 2002*, in: *Internat. Ser. Numer. Math.*, vol. 147, Birkhaeuser, 2004.
- [12] E. Bänsch, F. Haußer, O. Lakkis, B. Li, A. Voigt, Finite element method for epitaxial growth with attachment–detachment kinetics, *J. Comput. Phys.* 194 (2004) 409–434.
- [13] F. Haußer, A. Voigt, Weakly anisotropic surface diffusion, a numerical approach by parametric finite elements, Technical Report, SFB 611, Universität Bonn, 2003.
- [14] G. Dziuk, An algorithm for evolutionary surfaces, *Numer. Math.* 58 (6) (1991) 603–611.
- [15] A. Schmidt, K.G. Siebert, Albert — software for scientific computations and applications, *Acta Math. Univ. Comenianae* 70 (2001) 105–122.
- [16] K. Mikula, D. Ševčovič, Computational and qualitative aspects of evolution of curves driven by curvature and external force, *Comp. Visual. Sci.* 6 (2004) 211–225.
- [17] S.J. Watson, F. Otto, B.Y. Rubenstein, S.H. Davis, Coarsening dynamics of the convective Cahn–Hilliard equation, *Physica D* 178 (2003) 127–148.
- [18] S.J. Watson, Crystal growth, coarsening and the convective Cahn–Hilliard equation, in: A. Visintin, P. Colli, C. Verdi (Eds.), *Free Boundary Problems, Trento, 2002*, in: *Internat. Ser. Numer. Math.*, vol. 147, Birkhaeuser, 2004.